Creating Curvature Adapted Subdivision Control Meshes from Scan Data

Simon Kloiber[a] and Ursula H. Augsdörfer
Institute of Computer Graphics and Knowledge Visualisation,
Graz University of Technology, Inffeldgasse 16c, Graz, Austria

Keywords: Quad-dominant Remeshing, Surface Reconstruction.

Abstract: Often, designers have real-life models which need to be converted to a mathematical representation for further processing. For the designer to be able to manipulate the data sensibly and in a controlled manner the number of data points have to be reduced. However, if the new reduced representation of the shape is sparse everywhere, high frequency detail in the model will be lost. In this work we modify an existing quad meshing algorithm to convert a dense triangle mesh capturing the shape of the real-life model to a quad-dominant mesh of varying density. Our distribution of vertices allows to represent high frequency features in the surface, without increasing the density of the mesh elsewhere unnecessarily. Our quad mesh approximates the scan data up to a predefined error margin. This quad mesh is then transformed into a subdivision control mesh, which corresponds to a limit subdivision surface which closely resembles the scan data.

1 INTRODUCTION

Often, designers create real-life models of their ideas. The real-life model is then scanned to obtain a digital representation in form of a point cloud, which can be converted to a triangle mesh. Because these meshes closely capture the shape of the real-life models, we will refer to these dense triangular meshes as reference meshes. To be able to further refine the design within a design pipeline, a mathematical representation of the shape has to be found. Subdivision surfaces are able to model complex shapes with a single surface. They are defined by a coarse set of control points and a subdivision algorithm. To continue the design with subdivision surfaces, the reference mesh has to be converted into a subdivision control mesh. The extraction of an adaptive subdivision control mesh from dense triangle meshes is the focus in this paper. There are many different subdivision schemes resulting in limit surfaces with different mathematical properties. While the algorithm presented is applicable to any subdivision scheme, we will base all examples on the Catmull-Clark scheme since it is the de facto standard subdivision scheme in the CAD and entertainment industry. Catmull-Clark subdivision operates on quadrilateral meshes.

The paper is structured as follows. In Section 2 we discuss related work on the topic of quad mesh generation. In Section 3 we describe how we extend an existing algorithm for isotropic quad meshing to create non-uniform isotropic quad meshes that are sensitive to the curvature of the surface and adapt the size of the quadrilaterals such that the error of the extracted quad-dominant mesh to the reference mesh does not exceed a given threshold. We also describe a simple way to convert a given quadrilateral polyhedron to a Catmull-Clark control mesh so that the limit surface closely describes the shape captured in the reference mesh. We present our results in Section 4. We close with the conclusion in Section 5.

2 QUADRILATERAL MESHING

Because Catmull-Clark subdivision is based on a quadrilateral mesh, we first need to compute a quad mesh (also called *quadrangulation* or *quad meshing*) from a given input mesh. Quad meshing is a topic of interest in many applications, like texture mapping, parameterisation and finite element analysis and there are numerous different approaches and methods. A comprehensive survey is e.g. provided by (Bommes et al., 2013b).

Quad meshing methods either define parametrisa-

[a] https://orcid.org/0000-0003-1186-7630

Kloiber, S. and Augsdörfer, U.
Creating Curvature Adapted Subdivision Control Meshes from Scan Data.
DOI: 10.5220/0008989601490159
In *Proceedings of the 15th International Joint Conference on Computer Vision, Imaging and Computer Graphics Theory and Applications (VISIGRAPP 2020) - Volume 1: GRAPP*, pages 149-159
ISBN: 978-989-758-402-2; ISSN: 2184-4321

tions or curves, or employ triangle decimation to create quads. Parametrisations can be created through global optimisations (Ray et al., 2006; Hormann and Greiner, 2000; Kälberer et al., 2007; Bommes et al., 2009; Bommes et al., 2013a; Liu et al., 2011; Myles et al., 2010) or by defining a coarse layout of charts which are then parametrised (Tong et al., 2006; Dong et al., 2006; Zhang et al., 2010; Zhang et al., 2013). Another approach is defining curves on the reference mesh in a cross-based layout. Creating pure quad meshes is difficult with straightforward curve based approaches because additional structures are needed (Campen et al., 2012). Quad-dominant approaches integrating curves are more prevalent (Alliez et al., 2003; Marinov and Kobbelt, 2004; Dong et al., 2005). A third approach employs triangle mesh decimation (Lai et al., 2010), where quadrilateral faces are created by combining triangles, and makes use of the fact that creating a triangulation is easier than creating a quadrangulation.

Some of these approaches allow anisotropy and adapt the mesh density according to curvature: (Zhang et al., 2010) create their pure quad mesh via parametrising the quasi-dual Morse-Smale Complex of a standing wave function with manual size control. (Alliez et al., 2003) create quad-dominant meshes from genus-0, non-closed input meshes. They use a smoothed curvature tensor field to guide curves in anisotropic regions and point sampling in spherical regions. The layout of the curves (i.e. density, anisotropy, geometric accuracy) can be influenced manually. (Marinov and Kobbelt, 2004) create a parametrization on an arbitrary input mesh on which curvature lines are traced. The traced lines satisfy a manually set sampling density. (Dong et al., 2005) create a smooth harmonic scalar field over the mesh. They compute a gradient vector field and use a second vector field which is orthogonal to the gradient field to trace integral lines. The spacing of these lines is curvature sensitive and may be controlled manually. (Lai et al., 2010) remesh the given triangle mesh such that the density of the newly created triangle mesh adapts to curvature. They then perform a relaxation on the triangle mesh which aligns the edges of the triangles such that non-aligned edges can be dropped to form curvature aligned quads. (Kovacs et al., 2011) introduce an anisotropic metric to feature aligned and harmonic parametrisations. This improves the approximation quality of these isotropic approaches. The quad-dominant remeshing algorithm by (Jakob et al., 2015) creates isotropic uniform quad-dominant meshes through quick, local optimisation of a parametrisation from triangle or point cloud reference meshes.

The results of uniform quad meshing methods cannot create sparse subdivision control meshes that have a low approximation error. We present a non-uniform quad meshing method, which adapts the density of control points to the degree of detail present in the original surface. To ensure an accurate representation of surface features, we adjust the size of mesh elements to reflect curvature variations, but also aim to align the mesh with shape features. This is achieved by modifying the algorithm presented in (Jakob et al., 2015) to respect the curvature detail of the original scan data.

3 ADAPTIVE QUAD MESHING

This section provides a comprehensive guide through our changes to *Instant Meshes* (Jakob et al., 2015). We created a work-chain that is able to transform reference meshes into subdivision control meshes with densities based on the curvature information of the referenced surface. The local approach of optimising the parametrization used by *Instant Meshes* is ideal for using curvature information to shape the grid size locally around each vertex. By adapting the local grid size to the curvature of the shape we create a mesh with large similar sized regular quadrilateral faces in flat regions with low curvature, and small quadrilateral faces in high curvature regions in order to capture high frequency details in the model. We constrain the orientation field estimation and feed the edge lengths into the position field estimation. The resulting mesh is post-processed to guarantee manifoldedness, to align quads with ridges, and to improve the topology of flat areas. Finally, the extracted mesh is transformed into a subdivision control mesh such that its limit surface corresponds to the reference surface given by the reference mesh.

The following steps are performed to extract a quad-dominant subdivision control mesh with curvature-based densities:

1. Build a multi-resolution hierarchy of the mesh. For each hierarchy level, estimate the curvature, compute the scales, and detect ridge vertices.
2. Optimise the orientation field.
3. Optimise the position field.
4. Extract the mesh.
5. Perform mesh clean-up.
6. Perform mesh smoothing.
7. Create the subdivision control mesh.

Changes in the density of Catmull-Clark subdivision control meshes are difficult to achieve because of their quad-based nature. Transitions from low to high densities have to be done with care because they will introduce additional extraordinary vertices (EVs). An extraordinary vertex has a valency other than regular, that is either more or less than four. Typically, the EVs are avoided, since they are associated with curvature problems in the limit surface. In this work, however, we accept the appearance of EVs in order to capture shape information encapsulated in high frequency regions of the surface.

3.1 Curvature Estimation

There are two ways to estimate curvature on a piecewise linear mesh: Fitting parametric surfaces locally around each vertex or estimating curvature in a discrete sense based on the neighbourhood of a vertex (Petitjean, 2002; Gatzke and Grimm, 2006). Parametric surface fitting generally produces better results at the expense of computation time compared to other methods. Most discrete methods are linear in time because they compute sums over neighbours, but are more susceptible to noise (Gatzke and Grimm, 2006). We employ principal curvatures to fit a parametric surface, because they are more precise and uniform compared to other methods. The improved precision warranted the increased time complexity (a factor of three for an input mesh with 50000 vertices and 100000 faces).

The parametric surface fitting method of cubic order developed in (Goldfeather and Interrante, 2004) estimates principal curvature directions well and computes satisfying results. To estimate the principal directions and curvature, a cubic order B-spline patch is fitted onto the neighbourhood of a vertex. For this, neighbouring vertices are brought into a local coordinate frame to create a system of equations where the neighbours describe the shape of the parametric surface. We found a 2-ring neighbourhood works well. Every neighbouring point introduces three equations with one equation for the position and two equations for the normals. The least-squares solution of this system of linear equations is the Weingarten curvature matrix of the cubic surface. The Eigenvalues of this matrix are the principal curvatures and its Eigenvectors are the corresponding principal directions.

From the estimated curvature, we take the largest absolute principal curvature as our guide for edge lengths. This ensures that the highest frequency detail is always respected.

3.2 Curvature Averaging

The curvature information might not be as smooth as needed for good results. This may be due to noise in the reference mesh or multiple different features coming together in the mesh. To address these issues, we tried different averaging methods to achieve a smooth curvature distribution. We also tried different weighing schemes, either in order to increase the influence of high curvature regions or based on similarity (be it curvature or normal similarity). We found that uniform weights for all neighbours in a 2-ring neighbourhood produced the most consistent results.

3.3 Error Estimation and Edge Length

A scale parameter employed in the work of (Jakob et al., 2015) defines a global desired edge length of the extracted mesh. This scale influences the position field calculation and the extraction itself. In the position field, the scale defines the positional invariance points of the field while in the extraction it is used to classify edges and to remove unnecessary edges. To adjust scale based on curvature, the first step is unravelling the global scale by giving each point its own. The transformation of curvature to scale is a one-dimensional map and is very similar to a simple transfer function in volume rendering (Ljung et al., 2016).

All information necessary to define a desired edge length for a given vertex that fits the complexity of the underlying surface is provided by the curvature estimation. The relation of a tangent to the osculating circle provides an error metric. We can use it to estimate the error when moving along a curve in direction of the tangent direction away from the vertex. As illustrated in Figure 1, for a vertex v with curvature κ along a tangential curve on the surface, the osculating circle has radius $\frac{1}{|\kappa|}$. When we move away from the point along this curve by x, we denote the estimated distance to the curve as ε. Users can select the desired error, which drives the edge length computation.

(Alliez et al., 2003) have used a similar estimation that places the constructed edge such that its endpoints are on opposing sides of the circle (i.e. the vertex is its centre). This way, the same error ε will allow an edge length of $2x(\varepsilon)$. Their derivation creates edges that are larger and become smaller too slowly. Hence, the factor of two is not incorporated in our edge length computation.

Because the derived edge lengths tend to infinity as the curvature approaches zero, we cap edge lengths to remain smaller than five times the global edge length. In areas where the edge length is too

$$
\begin{aligned}
r &= \frac{1}{|\kappa|} \\
r^2 &= (r-\varepsilon)^2 + x^2 \\
x^2 &= r^2 - (r-\varepsilon)^2 \\
x^2 &= \frac{1}{|\kappa|^2} - (\frac{1}{|\kappa|} - \varepsilon)^2 \\
x^2 &= \frac{2}{|\kappa|}\varepsilon - \varepsilon^2 \\
\mathbf{x}(\varepsilon) &= \sqrt{\frac{2}{|\kappa|}\varepsilon - \varepsilon^2} \\
0 \leq \varepsilon &\leq \frac{1}{|\kappa|}
\end{aligned}
$$

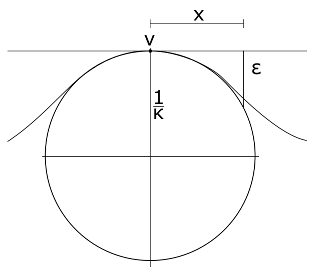

Figure 1: The derivation of the maximum edge length $\mathbf{x}(\varepsilon)$ with an error of ε, for tangential edges going out of vertex v with curvature κ.

small for the density of the reference mesh, the position field can either not form clusters or forms clusters that are too small to extract vertices. If not specified differently by a user, (Jakob et al., 2015) set the global edge length such that the expected number of extracted vertices is $1/16$th of the number of reference vertices. This expectation has become less precise due to varying quad sizes but is still a good indicator to ensure that edge lengths do not become too small. Setting the minimal edge length to be between 70% and five times the global edge length has proven to be a good estimate.

3.4 Hierarchy

The method in (Jakob et al., 2015) creates a multi-resolution hierarchy of the reference mesh to improve stability and convergence of the orientation and position field estimation. The lowest level of the hierarchy contains all vertices of the reference mesh. New levels of the hierarchy are created by merging pairs of vertices with the highest weights. Weights are calculated via the dot product of vertex normals, scaled by the relation of maximum over minimum area of their barycentric cells to ensure a balanced hierarchy tree.

The curvature on each level of the hierarchy is estimated based on the vertices and their adjacency. Since vertices are merged through averages, the higher level mesh might have areas with different curvatures than the original mesh. Whether the curvature information of higher levels resembles the curvature of the original mesh depends on the weighting that decides which points are supposed to be merged on each level.

3.5 Orientation Field Optimisation

While the orientation field computed in (Jakob et al., 2015) produces satisfying orientation fields, it is not without flaws. Especially for rotation symmetric objects, the algorithm cannot always direct the orientation field so that the flow lines align with feature lines (e.g. ridges, creases). To address this, we introduce constraints for vertices lying on feature lines based on their principal directions. It is important to note that these constraints have to be used with care because they may greatly disturb/constrain the orientation field optimisation. We use constraints from anisotropic regions of the mesh because the principal directions are well defined in these regions.

To classify highly anisotropic regions, a threshold for the difference between minimal and maximal curvature needs to be defined and the maximal curvature must exceed some extent to make sure the anisotropic region is on a feature line with high curvature in one direction. To classify anisotropy, we use a scale-invariant quotient (Rugis and Klette, 2006), which is computed from the principal curvatures, κ_1 and κ_2, and is computed as $\kappa_3 = \frac{\min(|\kappa_1|,|\kappa_2|)}{\max(|\kappa_1|,|\kappa_2|)}$. We define the threshold for high curvature by the median curvature of all principal curvatures for all vertices. The median of the curvature distribution is less affected by outliers but depends on the shape of the reference mesh and its distribution of curvature. It proved to be stable enough as a measure for high curvature. We can now define candidate vertices for feature lines to have $\kappa_3 < 0.1$ and $\max(|\kappa_1|,|\kappa_2|) > \text{median}$. Only one path of vertices is needed to constrain the orientation along a feature line but the candidate vertices are not limited to a single path yet. To remedy this, only vertices v, which have $\max(|\kappa_1^v|,|\kappa_2^v|) > \max(|\kappa_1^{v_i}|,|\kappa_2^{v_i}|)$ for each of its neighbours v_i and have at least one neighbour which is a feature candidate are true feature vertices. True feature vertices require a feature candidate neighbour to avoid stray feature candidates coming from noise in the curvature estimation. This classification is simple to compute and suffices to give a minimal set of constraints for the orientation field optimisation. The merits of classifying feature vertices and adding constraints to the orientation field optimisation can be seen in Figure 2.

3.6 Position Field Optimisation

The position field optimisation of the algorithm of (Jakob et al., 2015) calculates a local parametrization for every vertex. A positional vote for each vertex is calculated via a sum of positions of its neighbours. For each neighbour, an optimal position of the vertex

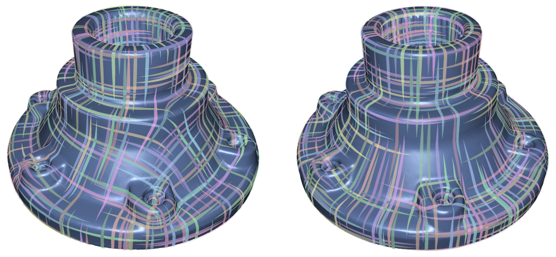
Figure 2: By adding a sparse set of constraints through the principal directions of vertices that lie on ridges, the orientation field optimisation is better aligned to surface features.

and the neighbour is calculated based on their associated edge length.

3.7 Extraction

The extraction of the final mesh is done in two stages: extracting a graph of vertices and their neighbourhood and then extracting a set of quad-dominant faces from this neighbourhood. The following three changes were made to the mesh extraction mechanism.

Minimal Vertex Cluster Size. In (Jakob et al., 2015) extracted vertices are discarded when the size of their cluster in the parametrization is smaller than $1/10$ of the average cluster of all extracted vertices to avoid stray extracted vertices. For most meshes, $1/10$ is appropriate. However, when the extracted mesh has large faces, the clusters of their vertices may distort the average such that vertex clusters are discarded that would still be needed. To give control over this behaviour, we added an option to change the fraction of the cluster size below which vertices are discarded.

Snapping Flat Triangles. When extracting vertices, the original method (Jakob et al., 2015) may produce skinny triangles (Botsch and Kobbelt, 2002). These triangles may cause problems during subsequent processing stages of the mesh. As in the original work, we change their neighbourhood and positioning so they form a line instead of a triangle.

In (Jakob et al., 2015) three neighbouring vertices are considered a skinny triangle if the length of any edge of the triangle is below 30% of the global edge length scale. However, since the scale is not global anymore, this threshold does not work and each extracted vertex needs its own scale. The new scales for the extracted vertices are based on the scales of the vertices which contribute to their position in the position field parametrization. They are computed as a weighted sum over all scales of contributing vertices, using the same weights as the computation of the extracted vertex positions. We define the new threshold for skinny triangles to be the sum of 10% of each extracted vertex' scale. It is equivalent to the original threshold when all vertices have the same scale.

If a skinny triangle is encountered, the vertex for which the scale was calculated is moved. If this vertex is close to one of the other two vertices of the triangle then these two are merged and their position is averaged. When the vertex to be moved is not close to any of the other vertices forming the triangle it is moved so that all three vertices are collinear. Unfortunately, this simple threshold is sometimes moving vertices away from feature lines of the reference mesh, which decreases the quality of the mesh.

To prevent bad snapping, we set the position of merged vertices to be the position of the vertex with greater principal curvature instead of computing an averaged position. Collinear snapping is only performed if the extracted vertex to be moved does not lie on a feature line (i.e., it has less than two contributing input feature vertices) or all three vertices of the extracted triangle lie on a feature line (i.e., more than one feature vertex).

Creating Quads. When extracting faces, the algorithm of Jakob et al. (Jakob et al., 2015) searches for polygons in the adjacency graph of the extracted vertices. A face is created if the polygon is a triangle, a quad or a pentagon. Selecting quads for filling n-gons follows a greedy scoring system. For an n-gon $v_0, v_1, \ldots, v_{n-1}$, the score is calculated as a sum of differences between the four next angles' and a right angle, starting from i:

$$score_i = \sum_{j=0}^{3} |90^{\circ} - \measuredangle(v_1 v_2 v_3)|$$

where $v_1 = v_{i+j \pmod n}$, $v_2 = v_{i+j+1 \pmod n}$, and $v_3 = v_{i+j+2 \pmod n}$.

In (Jakob et al., 2015), no reasoning for this scoring is given and it does not try to find perfect quads as only the first two angles (i.e. $j = 0, j = 1$) are part of the quad.

To favour optimal quads, we use a new scoring system which does not use four consecutive angles but the four angles of the quad in question. We therefore define the score as above but use the following expressions for the angles: $v_1 = v_{i+j \pmod n}$, $v_2 = v_{i+(j+1 \pmod 4) \pmod n}$, and $v_3 = v_{i+(j+2 \pmod 4) \pmod n}$.

This scoring now fills the space with the most rectangular quad first. Observations on the behaviour suggest that the best quads are also well aligned with the principal directions and that no additional consideration for this alignment is necessary.

3.8 Ensuring Manifoldness

Because of the local nature of the position field optimisation and the greedy face creation, extracting a manifold quad-dominant mesh is not always possible. To remove the non-manifold parts of the mesh, Jakob et al. perform two passes where faces introducing non-manifold edges and then all faces surrounding non-manifold vertices are deleted. However, deleting affected faces results in holes. We changed the algorithm presented in (Jakob et al., 2015) to repair non-manifoldness instead of deleting it. Non-manifold normals (i.e. neighbouring faces with opposite normals) are not created during the extraction and do not need to be handled.

Non-manifold Edges. Non-manifold edges can be detected in the directed edge data-structure (Campagna et al., 1998) used to represent the extracted mesh, when the same directed edge is introduced by two faces. Removal of these edges is done by changing the affected faces or by removing one face. The method to repair a non-manifold edge is as follows: delete all vertices in both faces which are not part of the non-manifold edge and are adjacent to only one or two faces in total. If no vertex is deleted, delete one face as a last resort (if the non-manifold edge is a diagonal on one face, delete this face - otherwise delete a random face). When the deleted vertices leave faces with 2 or fewer vertices, they are deleted as well.

Non-manifold Vertices. Non-manifold vertices can be detected by creating a list of all faces adjacent to the vertex, starting at a random neighbouring face, traversing the neighbourhood of the vertex and removing all encountered faces off the list. If the vertex is non-manifold, it has more than one neighbouring face loop. So, if the list is not empty after all faces were visited, the vertex is non-manifold. To find all loops, this loop-search is repeated until all neighbouring faces have been assigned to a face loop. For each additional face loop, a new vertex is created and all instances of the non-manifold vertex are positioned to be the average of all adjacent vertices in their respective face loop.

While this method removes all non-manifold elements, it cannot guarantee that no holes are created, because there are cases where faces cannot be changed and must be deleted to ensure manifoldness. Since our goal is a closed mesh, the algorithm described in Section 3.7 is used to find and patch potential holes. To ensure that the hole-filling does not introduce non-manifoldness, one more iteration of non-manifold clean-up is performed.

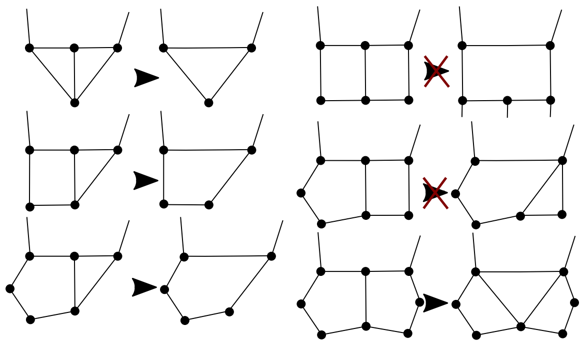
Figure 3: The cases considered in the elimination of T-junctions in the mesh as described in Section 3.9. Not all cases improve the quality of the mesh: Combining two quads (top right) is not feasible because this would introduce more non-quadrilateral faces to the mesh. Combining a quad and a 5-gon (second right) would create a triangle and a 5-gon, which is not favourable as well. While two 5-gons are possible in theory, it has not occurred during yet.

3.9 Mesh Post-processing

After the non-manifold clean-up, the extracted mesh still has potential for improvement. The following three additional passes for optimisation are performed.

Eliminating T-junctions. T-junctions in the extracted mesh induce extraordinary vertices in the subdivision control mesh. We can avoid T-junctions by altering the topology of the mesh as shown in Figure 3. To prevent losing detail, the two faces on either side of the edge ending in a T-junction must lie on similar planes and their edges adjacent to the T-vertex must lie, approximately, on a line. For the purposes of this clean-up, two faces lie on similar planes when their normals differ by less than five degrees. Two outgoing edges from the T-vertex lie on similar lines when the angle α between them is $175° < \alpha < 185°$. These angles have shown to be a fitting threshold. Figure 3 shows the different combinations of faces and their resolved topology. This elimination of T-junctions tends to reduce the number of non-quads and reduces the number of extraordinary vertices in the subdivision control mesh by one.

Feature Aligned Quad Edges. To ensure alignment of edges with surface features, two different approaches are used: The mis-aligned quad face is split into two triangles along the face diagonal closest to the feature or the quad face is removed by merging both endpoints of the diagonal on the feature line along the middle of the diagonal. Although removal does not introduce non-quads, it must be done with caution, because the quad may lie on a high curvature part of the feature line and removing it could increase the error to the reference mesh. Hence, only quads where the diagonal has a pair of adjacent edges which lie on a common line are removed, and all others are split into two triangles. We consider a pair of outgoing edges from both ends of the diagonal to be on the same line if, as before, the angle α between the edges is $175° < \alpha < 185°$. This angular threshold was determined empirically through observations over all compared meshes.

Finding these quads is a delicate task because false-positives must be avoided. We used the following criteria as a classification of mis-aligned quads:

- The average angle between the orientation field of both end-vertices and the face diagonal (with 90° rotation symmetry) must be smaller than 15°.
- The angle of the two triangles on both sides of the diagonal on the feature must be greater than 50°.
- The average largest principal curvature of both end-vertices of the diagonal must be greater than the curvature of the other face diagonal.
- The closest face of the reference mesh must be closer to the middle of the face diagonal than the middle of the other diagonal.

The first three criteria make sure that only quads on sharp feature lines are considered. The fourth criteria excludes false-positives where the removal or split would be performed on the wrong diagonal and thus worsening the result.

This post-processing improves the feature alignment of the extracted mesh. Edges follow the feature lines again and when a quad is removed, the endpoints of the diagonal are combined. The outcome of both approaches of ensuring feature alignment are shown in Figure 4.

Flat Neighbouring Triangles. We further reduce the number of non-quad faces in the mesh by merging neighbouring triangles which lie on a similar plane. This post-processing is applied before and after eliminating T-junctions and aligning edges with features. Two triangles are considered lying on a similar plane based on the same threshold as in Section 3.9.

3.10 Smoothing

The position field optimisation does not always produce perfect quads. Especially in areas where large edge lengths meet short edge lengths, some quads might be very distorted. To improve the quality of distorted quads without losing detail, tangential smoothing is performed. New vertex points are computed by averaging over all neighbours in a 1-ring neighbourhood and then projecting them onto the tangential plane of the original vertex. To preserve the features of the mesh, vertices are not smoothed when the largest angle between the normals of their neighbouring faces is greater than 50°. Three iterations of smoothing are able to restore distorted quads while largely preserving the difference in edge length.

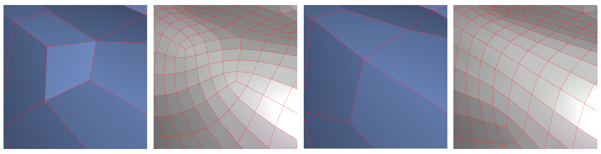
(a) Quad to be removed (b) After quad removal

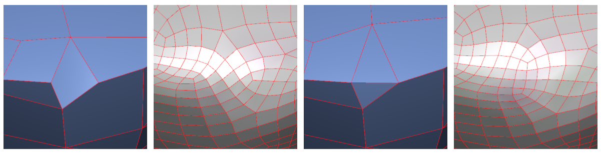
(c) Quad to be split (d) After quad split

Figure 4: The meshes and their corresponding subdivision meshes are shown before and after post-processing to avoid mis-aligned edges. Figures (a) and (c) show meshes with mis-aligned edges together with their corresponding subdivision mesh. Figures (b) and (d) show the meshes together with their subdivision meshes after post-processing. The ridge lines are kept intact by removing or splitting the quads as described in Section 3.9.

3.11 Subdivision Control Mesh

The next step is creating a Catmull-Clark subdivision control mesh from the extracted quad-dominant mesh. A subdivision control mesh is created via iteratively moving the vertices of the quad-dominant mesh along their normal until the limit point closely approximates the input mesh as described previously in (Thaller et al., 2016). The algorithm to derive a subdivision control mesh from a polygon mesh is as follows:

```
$mesh \leftarrow$ output of instant meshes
while Less than 20 iterations do
    for all vertices $\in$ mesh do
        $LimitPoint \leftarrow$ limit point of vertex
        $I \leftarrow$ intersection of reference mesh and Ray[$LimitPoint$, normal]
        $NewVertexPos \leftarrow vertex + (I - LimitPoint)$
    end for
    if $\max_{v \in mesh} |NewVertexPos - OldVertexPos| < \varepsilon$ then
        break
    end if
    $mesh \leftarrow$ all $NewVertexPos$
end while
```

The algorithm stops either after 20 iterations or when the maximum distance between old and new positions for vertices are below a threshold ε. Our ε is $10^{-4}\times$ the greatest dimension of the reference meshes bounding box.

To apply this algorithm, the limit points of the extracted mesh need to be calculated. Catmull-Clark subdivision surfaces correspond to bi-cubic B-splines in the regular region. In non-regular regions, for vertices with valences not equal to four, (Halstead et al., 1993) have derived a linear combination to compute the limit points from the control points.

4 RESULTS

The meshes resulting from our work are able to represent reference meshes up to a user-defined desired error, with an emphasis on distributing vertices so that high frequency details are preserved.

A change in density in quad meshes leads to vertices with a valence different to four or to the introduction of non-quads. Therefore, our resulting quad-dominant meshes have more extraordinary vertices compared with other approaches. They have uniform quads in regions of similar curvature of the reference mesh and adapt to changes in curvature with non-quads or EVs. The number of EVs and non-quads of our method depends on the number of transitions between low and high curvature regions because quad-dominant meshes need non-quads or EVs to make the corresponding transition of edge lengths.

Most isotropic approaches aim for pure quad or quad-dominant meshes while trying to minimise the number of EVs. This limits their abilities to adapt to curvature. Compared to our method, the isotropic meshes of Jakob et al. (Jakob et al., 2015) are more regular with fewer EVs and non-quads, and have quads with better quality. However, they are less dense in high curvature regions and thus cannot represent high frequency detail as well (c.f. Figure 5). Additionally, due to the dependence on curvature estimation, our approach is slower, but still interactive (timings with 16GB RAM, Intel i7-4930K CPU):

#Input Vertices	Jakob et al. (ms)	Our work(ms)
14000	500	1300
50000	850	2700
100000	1300	4600

To compare the original work of Jakob et al. and our contribution, we extracted meshes with a similar number of vertices through both approaches. We used the default setting for the original work but changed the desired number of extracted vertices to match our resulting meshes. Since the algorithm can only be set to approximate a number of vertices, we cannot compute the exact same number of vertices for both approaches. Both types of meshes were converted to subdivision control meshes. A visual comparison of the resulting subdivision surfaces demonstrates clearly how the algorithm presented in this paper is able to capture high frequency details present in the original data with a similar number of vertices.

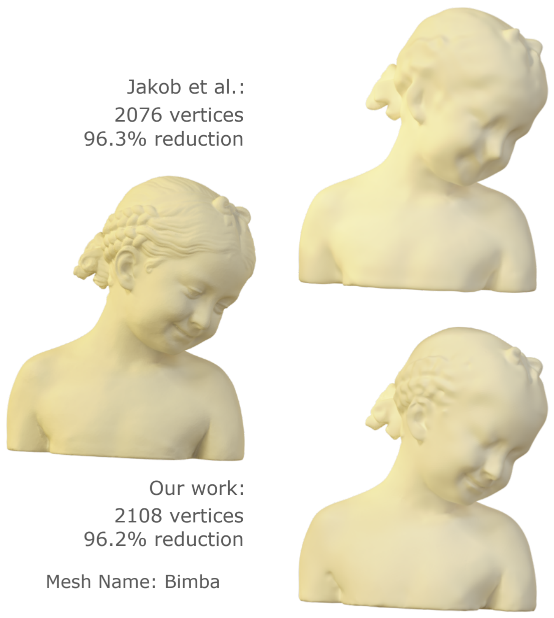

Figure 5: Comparison of subdivision surfaces for the original work (top) and our method (bottom) with a high density and the rendered original scan data (left).

To quantify the improvement, we employ a number of error metrics to compare subdivision surface derived using the approach presented in this paper to those derived from quad meshes using Jakob et al.'s approach. Averaged over all meshes compared in this paper, the following error can be observed:

Error Metric	EV's	Hausdorff Distance	Avg. Quad Quality	Avg. Face Centroid Dist.
Jakob et al.	0.28%	0.468	0.489	0.122
Our algorithm	0.89%	0.463	1.291	0.115
% Difference	+246.01%	-2.90%	+180.79%	-6.06%

Here, the average quad quality is an adapted quad quality measure taken from (Marinov and Kobbelt, 2006) and the average face centroid distance to the reference mesh is used to avoid large quads in detailed regions. The adaptation of the quad quality measure comes from omitting the deviation from a square, since our goal is not a perfect isotropic mesh.

The introduced curvature-dependent vertex densities improve the Hausdorff distances between limit surface and reference mesh. It also shows how the focus on adaptive edge length increases the number

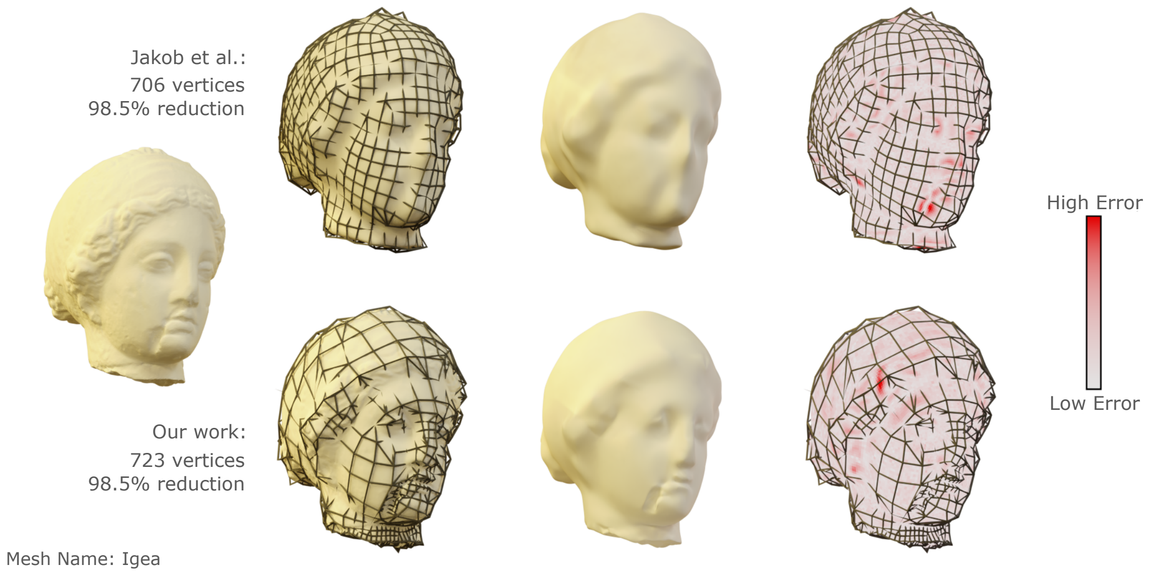

Figure 6: On the left is the rendered input mesh resulting from scan capture. 2nd from left: The subdivision control mesh generated from the scan data. The limit surface derived from control mesh is shown 3rd from left. On the right we used colour to highlight the error between the scan data and the subdivision limit surface. Our algorithm creates a control mesh which is dense in regions where it is required to capture fine detail, but coarse in regions of low curvature (bottom row). The resulting limit surface captures high frequency features at a considerably higher precision opposed to the original approach by Jakob et al., who are more concerned with regularity of the underlying mesh. Despite a similar number of vertices, our algorithm captures the scar around the mouth quite well, while using a coarse grid in regions with less detail.

of extraordinary vertices and deteriorates quad quality. Additionally, the proposed algorithm struggles when two very flat areas meet at a sharp crease. The problem arises from the very concentrated high curvature region of the sharp crease being surrounded by nearly zero curvature. When the disparity between large edge lengths and small edge lengths is too sudden, the position field optimisation may not produce optimal results. To tackle this, however, curvature can either be smoothed stronger for more gradual curvature changes, or the desired error can be set lower to create smaller quads overall.

Figure 6 and Figure 7 compare the different meshes and errors between the original and our approach. They show the improved accuracy in detailed regions and more irregular meshes that our curvature adapted edge lengths produce, when compared to the isotropic approach in (Jakob et al., 2015). Figure 8 compares the results of both approaches for a variety of meshes. The most notable differences are in regions with fine detail.

All our additional methods and many options for the behaviour of the algorithms are added to the software created in (Jakob et al., 2015). With the embedded batch mode, a user may extract quad-dominant or subdivision control meshes quickly based on our set of default options. Because of the variety of options, it is also possible to find a set of parameter setting to obtain improved results for specific meshes. Because the extraction is fast and initialisation is random, trying different options to find good solutions is easy.

5 CONCLUSION

We have created an adaptive quad-dominant meshing method with a focus on curvature-dependent density to accurately capture high frequency detail in the original data. A subsequent conversion of the extracted quad meshes to subdivision control meshes yields subdivision surfaces that faithfully describe even detailed features of the original shape. Possible defects in the parametrisation have been addressed through post-processing steps. Our algorithm presented in this paper enables the creation of coarse subdivision control meshes with corresponding subdivision limit surfaces which precisely model arbitrary shapes with a low number of vertices, while still accurately representing the reference shape, by offering higher density of the control mesh in regions with detailed features. The trade-off, however, is higher irregularity of the derived subdivision control mesh.

The design is very flexible and may be adapted to more specialised applications. Our focus was on an automated process that is able to produce satisfying results for a variety of inputs. Further work may

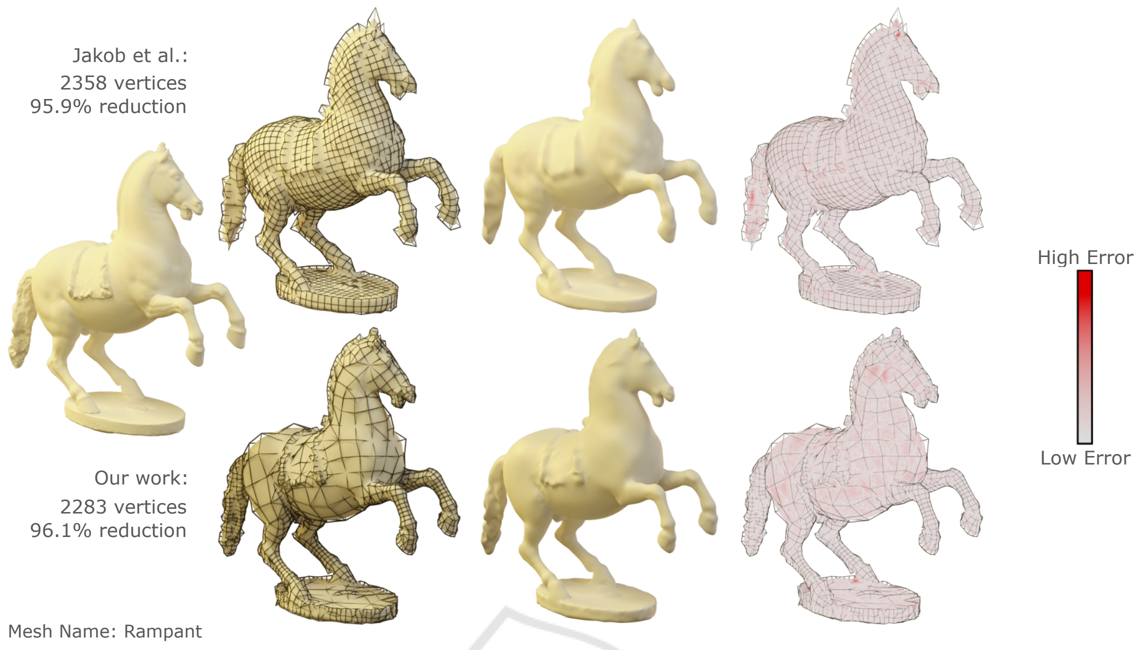

Figure 7: Same setup as Figure 6. We can see that the high frequency areas are better preserved with out approach (bottom), however, low frequency areas around the neck and behind the saddle lose some detail as their curvature is too low. This shows how our method distributes the expected error more evenly over the mesh, while still maintaining a low number of vertices.

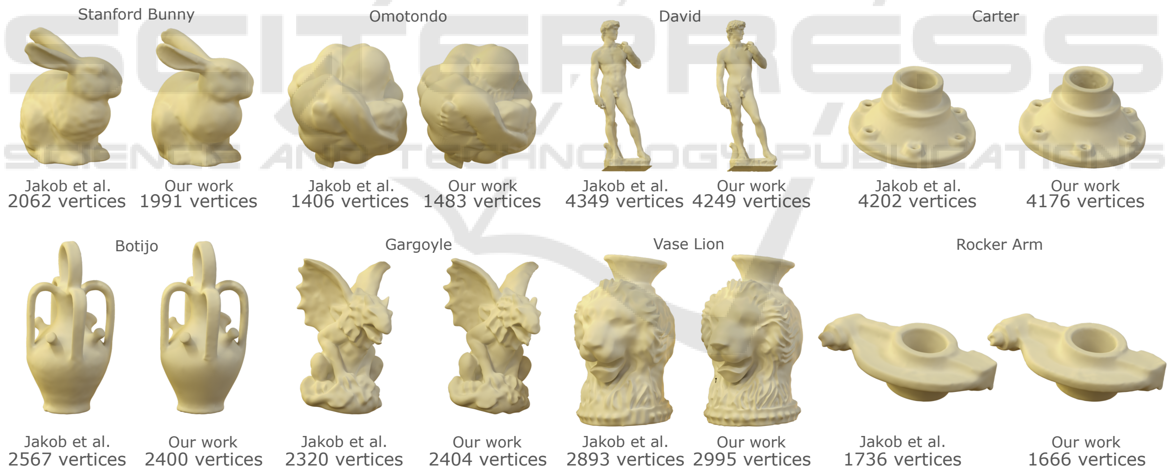

Figure 8: An overview over a variety of resulting subdivision meshed for both approaches and the mesh names. Vertex numbers represent the extracted control meshes that were used to generate the subdivision meshes. All input meshes were taken from the supplementary material of (Jakob et al., 2015).

include more post-processing to ensure that the extracted meshes fulfil the demands of more specific applications, more specialised settings for a subset of meshes or different constraints on the parametrisation.

REFERENCES

Alliez, P., Cohen-Steiner, D., Devillers, O., Lévy, B., and Desbrun, M. (2003). Anisotropic polygonal remeshing. *ACM Transactions on Graphics*, 22(3):485.

Bommes, D., Campen, M., Ebke, H.-C., Alliez, P., and Kobbelt, L. (2013a). Integer-grid maps for reliable quad meshing. *ACM Transactions on Graphics*, 32(4):1.

Bommes, D., Lévy, B., Pietroni, N., Puppo, E., Silva, C., Tarini, M., and Zorin, D. (2013b). Quad-mesh generation and processing: A survey. *Computer Graphics Forum*, 32(6):51–76.

Bommes, D., Zimmer, H., and Kobbelt, L. (2009). Mixed-integer quadrangulation. *ACM Transactions on Graphics*, 28(3):1.

Botsch, M. and Kobbelt, L. (2002). A robust procedure to eliminate degenerate faces from triangle meshes. *Proc. of Vision, Modeling, and Visualization 01*.

Campagna, S., Kobbelt, L., and Seidel, H.-P. (1998). Directed Edges - A Scalable Representation for Triangle Meshes. *Journal of Graphics Tools*, 3(4):1–11.

Campen, M., Bommes, D., and Kobbelt, L. (2012). Dual loops meshing. *ACM Transactions on Graphics*, 31(4):1–11.

Dong, S., Bremer, P.-T., Garland, M., Pascucci, V., and Hart, J. C. (2006). Spectral surface quadrangulation. *ACM Transactions on Graphics*, 25(3):1057.

Dong, S., Kircher, S., and Garland, M. (2005). Harmonic functions for quadrilateral remeshing of arbitrary manifolds. *Computer Aided Geometric Design*, 22(5):392–423.

Gatzke, T. D. and Grimm, C. M. (2006). Estimating Curvature on Triangular Meshes. *International Journal of Shape Modeling*, 12(01):1–28.

Goldfeather, J. and Interrante, V. (2004). A novel cubic-order algorithm for approximating principal direction vectors. *ACM Transactions on Graphics*, 23(1):45–63.

Halstead, M., Kass, M., and DeRose, T. D. (1993). Efficient, fair interpolation using Catmull-Clark surfaces. In *Proceedings of the 20th annual conference on Computer graphics and interactive techniques - SIGGRAPH '93*, SIGGRAPH '93, pages 35–44, New York, NY, USA. ACM.

Hormann, K. and Greiner, G. (2000). Quadrilateral remeshing. In *Proceedings of Vision, Modeling and Vizualization, 2000*, pages 153–162.

Jakob, W., Tarini, M., Panozzo, D., and Sorkine-Hornung, O. (2015). Instant field-aligned meshes. *ACM Transactions on Graphics*, 34(6):1–15.

Kälberer, F., Nieser, M., and Polthier, K. (2007). QuadCover - Surface Parameterization using Branched Coverings. *Computer Graphics Forum*, 26(3):375–384.

Kovacs, D., Myles, A., and Zorin, D. (2011). Anisotropic quadrangulation. *Computer Aided Geometric Design*, 28(8):449–462.

Lai, Y. K., Kobbelt, L., and Hu, S. M. (2010). Feature aligned quad dominant remeshing using iterative local updates. *CAD Computer Aided Design*, 42(2):109–117.

Liu, Y., Xu, W., Wang, J., Zhu, L., Guo, B., Chen, F., and Wang, G. (2011). General planar quadrilateral mesh design using conjugate direction field. *ACM Transactions on Graphics*, 30(6):1.

Ljung, P., Krüger, J., Groller, E., Hadwiger, M., Hansen, C. D., and Ynnerman, A. (2016). State of the Art in Transfer Functions for Direct Volume Rendering. *Computer Graphics Forum*, 35(3):669–691.

Marinov, M. and Kobbelt, L. (2004). Direct anisotropic quad-dominant remeshing. In *Proceedings - Pacific Conference on Computer Graphics and Applications*, PG '04, pages 207–216, Washington, DC, USA. IEEE Computer Society.

Marinov, M. and Kobbelt, L. (2006). A robust two-step procedure for quad-dominant remeshing. *Computer Graphics Forum*, 25(3):537–546.

Myles, A., Pietroni, N., Kovacs, D., and Zorin, D. (2010). Feature-aligned T-meshes. *ACM SIGGRAPH 2010 papers on - SIGGRAPH '10*, (July 2010):1.

Petitjean, S. (2002). A survey of methods for recovering quadrics in triangle meshes. *ACM Computing Surveys*, 34(2):211–262.

Ray, N., Li, W. C., Lévy, B., Sheffer, A., and Alliez, P. (2006). Periodic global parameterization. *ACM Transactions on Graphics*, 25(4):1460–1485.

Rugis, J. and Klette, R. (2006). A scale invariant surface curvature estimator. *Lecture Notes in Computer Science (including subseries Lecture Notes in Artificial Intelligence and Lecture Notes in Bioinformatics)*, 4319 LNCS:138–147.

Thaller, W., Augsdörfer, U., and Fellner, D. W. (2016). Procedural mesh features applied to subdivision surfaces using graph grammars. *Computers and Graphics (Pergamon)*, 58:184–192.

Tong, Y., Alliez, P., Cohen-Steiner, D., and Desbrun, M. (2006). Designing Quadrangulations with Discrete Harmonic Forms. In *Eurographics Symposium on Geometry Processing*, SGP '06, pages 201–210, Aire-la-Ville, Switzerland, Switzerland. Eurographics Association.

Zhang, M., Huang, J., Liu, X., and Bao, H. (2010). A wave-based anisotropic quadrangulation method. *ACM Transactions on Graphics*, 29(4):1.

Zhang, M., Huang, J., Liu, X., and Bao, H. (2013). A divide-and-conquer approach to quad remeshing. *IEEE Transactions on Visualization and Computer Graphics*, 19(6):941–952.